

## Article

# Biocompatible Fe-Based Metal-Organic Frameworks as Diclofenac Sodium Delivery Systems for Migraine Treatment

Aleksandra Galarda and Joanna Goscianska \* 

Faculty of Chemistry, Department of Chemical Technology, Adam Mickiewicz University, Uniwersytetu Poznańskiego 8, 61-614 Poznań, Poland; aleksandra.galarda@amu.edu.pl

\* Correspondence: asiagosc@amu.edu.pl

**Abstract:** Migraine is now the sixth most common disease in the world and affects approximately 15% of the population. Non-steroidal anti-inflammatory drugs, including ketoprofen, diclofenac sodium, and ibuprofen, are often used during migraine attacks. Unfortunately, their efficiency can be reduced due to poor water solubility and low cellular uptake. This requires the design of appropriate porous carriers, which enable drugs to reach the target site, increase their dissolution and stability, and contribute to a time-dependent specific release mode. In this research, the potential of the MIL-88A metal-organic frameworks with divergent morphologies as diclofenac sodium delivery platforms was demonstrated. Materials were synthesized under different conditions (temperature: 70 and 120 °C; solvent: distilled water or N,N-Dimethylformamide) and characterized using X-ray diffraction, low-temperature nitrogen adsorption/desorption, thermogravimetric analysis, infrared spectroscopy, and scanning electron microscopy. They showed spherical, rod- or diamond-like morphologies influenced by preparation factors. Depending on physicochemical properties, the MIL-88A samples exhibited various sorption capacities toward diclofenac sodium (833–2021 mg/g). Drug adsorption onto the surface of MIL-88A materials primarily relied on the formation of hydrogen bonds, metal coordination, and electrostatic interactions. An in vitro drug release experiment performed at pH 6.8 revealed that diclofenac sodium diffused to phosphate buffer in a controlled manner. The MIL-88A carriers provide a high percentage release of drug in the range of 58–97% after 24 h.

**Keywords:** MOFs; morphology control; drug delivery platforms; anti-migraine therapy; non-steroidal anti-inflammatory drug adsorption; two-stage drug release



**Citation:** Galarda, A.; Goscianska, J. Biocompatible Fe-Based Metal-Organic Frameworks as Diclofenac Sodium Delivery Systems for Migraine Treatment. *Appl. Sci.* **2023**, *13*, 12960. <https://doi.org/10.3390/app132312960>

Academic Editors: Gianpiero Calabrese and Antonia Mancuso

Received: 10 November 2023

Revised: 29 November 2023

Accepted: 1 December 2023

Published: 4 December 2023

**Correction Statement:** This article has been republished with a minor change. The change does not affect the scientific content of the article and further details are available within the backmatter of the website version of this article.



**Copyright:** © 2023 by the authors. Licensee MDPI, Basel, Switzerland. This article is an open access article distributed under the terms and conditions of the Creative Commons Attribution (CC BY) license (<https://creativecommons.org/licenses/by/4.0/>).

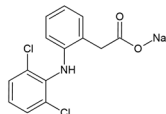
## 1. Introduction

Migraine is one of the most common neurological illnesses, characterized by episodic, severe headache attacks, typically lasting between 4 to 72 h. It impacts approximately 14–15% of the worldwide population, including two to three times more females than males [1,2]. Headaches often occur in adults aged 20 to 50, but children and adolescents are also subjected [2]. In addition to a higher incidence of migraines, women declare longer attack durations and recovery times, as well as greater disability [3]. This gender disparity suggests that hormonal factors, particularly estrogen levels, play a significant role in migraine, as women often report changes in their headache patterns concerning their menstrual cycle [2,4]. Migraine is identified by additional symptoms such as phonophobia and photophobia, episodes of vomiting, diarrhea, and nausea [5]. Moreover, approximately 15–30% of people suffering from migraine experience headaches with an aura, which is a neurological phenomenon characterized by sensory, visual, and occasionally language disorders [6]. This increases the risk of many conditions, such as stroke and other cardiovascular diseases [7]. It was also observed that people with chronic migraines complain about insomnia and fatigue. Treatments for such symptoms include taking acute and preventive drugs. Multiple medications are effective in the immediate management of migraine episodes, e.g., non-steroidal anti-inflammatory drugs (NSAIDs, i.e., naproxen

sodium, ibuprofen, ketoprofen, and diclofenac sodium), analgesics (i.e., paracetamol), triptans (sumatriptan, zolmitriptan, eletriptan, and rizatriptan), and calcitonin gene-related peptide (CGRP) receptor antagonists [8]. Conventional drug dosage forms (tablets, capsules, granules, etc.) are characterized by various limitations. The main concern is the potential for side effects such as renal dysfunction, gastrointestinal bleeding, and cardiovascular events [9]. It could be problematic in the case of taking drugs over an extended period at high doses. Many active pharmaceutical ingredients often have low solubility as well as poor absorption ability from the site of administration [10]. When drugs are ingested, the acidic conditions in the digestive system, along with the presence of digestive enzymes, can lead to their degradation before they can reach the bloodstream [11]. Given this, there is a necessity to develop an optimized drug delivery platform that will carry and liberate the pharmaceuticals at a controlled rate and maintain the desired therapeutic effect for a longer time [12,13]. Controlled and sustainable drug release platforms are one of the most rapidly advancing science topics due to their influence on human health. They can extend the pharmacological action duration of drugs, reduce the frequency of dosage, and consequently prevent the occurrence of adverse effects [14,15]. So far, a wide variety of ordered mesoporous silica, carbon materials, polymeric, and hybrid structures have been designed as targeted and controlled drug delivery systems [16–19]. Among them, metal-organic frameworks (MOFs), an interesting class of crystalline materials developed by linking molecular building blocks into a predetermined, extended periodic structure, found biomedical applications [20]. They have been investigated for drug delivery in recent years due to their high adsorption capacity, biocompatibility, and biodegradation [21]. Additionally, they are able to reach precise and sustained drug release. One of the most popular MOFs for drug delivery applications is those synthesized at the Lavoisier Institute known as MIL (MIL—Matériaux de l'Institut Lavoisier) materials [22]. They consist of iron nodes, naturally present in the body, which reduces their toxicity [23]. This group includes, i.e., MIL-88A, MIL-101(Fe), MIL-100(Fe), and MIL-53(Fe). Almáši and co-workers [24] successfully used MIL-101(Fe) functionalized with various polyamines as a naproxen sodium carrier. They reported 91.1% of drug release from MIL-101(Fe)-NH<sub>2</sub> at pH 7.4 after 24 h. Gordon et al. [25] incorporated acetaminophen into MIL-53(Fe), which was slowly liberated under simulated physiological conditions. It was found that 100% of the drug was released within 6 days. MIL-88A has been the subject of much research in the last decade as an adsorbent, catalyst, and energy harvester [26–30]. Its biocompatibility, low toxicity, easy synthesis via solvo/hydrothermal methods, and flexible structure render it an ideal candidate for drug hosting [26]. It is composed of non-toxic iron ions and fumaric acid—an endogenous linker and an important intermediate metabolite in the Krebs cycle [31]. In the case of its degradation in the body, the linker is metabolized, which decreases the risk of adverse effects (LD<sub>50</sub> (Fe) = 30 g/kg, LD<sub>50</sub> (fumaric acid) = 10.7 g/kg; LD—lethal dose) [23,32]. The *in vitro* and *in vivo* cytotoxicity of MIL-88A was investigated in several studies. In Horcajada and co-workers' research [32], 150 mg/kg/day of MIL-88A was injected into the rat liver and spleen for 4 days. After 10 days, there was no result in detectable toxicity. Baati et al. [31] examined the *in vivo* acute toxicity of high doses (up to 220 mg/kg) of MIL-88A nanoparticles. After intravenous administration, the liver and spleen maintained their functionality without any indications of enduring toxicity, displaying only temporary anomalies. Wuttke and co-workers [33] synthesized iron(III) fumarate nanoparticles under different conditions and carried out toxicity and cell association experiments. It was found that at concentrations up to 200 µg/mL, different forms of MIL-88A samples did not induce distinct impacts on cell viability within 24 h of exposure. The lack of immune or inflammatory responses following the administration of MIL-88A materials indicates their non-toxic nature [32]. MIL-88A was used as a carrier of different drugs and biologically active gases. McKinlay et al. [34] utilized MIL-88(Fe) materials for nitric oxide adsorption and delivery. The results showed a substantial NO release at the biological level for prolonged periods. Kim and co-workers [35] examined NH<sub>2</sub>-MIL-88(Fe) as a carrier for brimonidine. The drug was encapsulated at a concentra-

tion of 121.3  $\mu\text{g}/\text{mg}$  and liberated in a controlled manner over 12 h. Darvishi et al. [36] synthesized MIL-88(Fe) material on the surface of the carboxymethyl cellulose and used it as a delivery platform for a widely prescribed antibiotic: tetracycline. The sustained release of 64.3% tetracycline took place over 384 h. Wuttke and co-workers [37] coated MIL-88A with 1,2-dioleoyl-sn-glycero-3-phosphocholine (DOPC)-derived liposomes and applied it as irinotecan, floxuridine, and a Suberoyl bis-hydroxamic acid delivery system. The experiments demonstrated that the liposome-coated MIL-88A (Lip-MIL-88A) platform facilitated intracellular drug release, which could improve cancer treatment. Nevertheless, there is a lack of existing literature on the utilization of MIL-88A as a carrier of diclofenac sodium (DS), a phenylacetic acid widely used during migraine attacks. In addition, this drug is also employed in the management of lupus, rheumatic fever, psoriatic and rheumatoid arthritis, and gout [38]. Table 1 outlines the physicochemical properties and structure of DS. Diclofenac sodium is available on the market, mainly in the form of tablets, capsules, or gels. After oral administration, the bioavailability of the drug and its plasma half-life are approximately 50–60% and 1–2 h, respectively [39]. The necessity for multiple daily doses of this medication can lead to adverse outcomes, including gastrointestinal upset, increased risk of cardiovascular events, drug-induced hepatic damage, or diarrhea [40]. Hence, our study aimed to optimize the synthesis of non-toxic Fe-based metal-organic frameworks, MIL-88A, with divergent morphologies and their application as carriers in the diclofenac sodium release at the medium reflecting intestinal condition (pH 6.8).

**Table 1.** Physicochemical properties of diclofenac sodium.

Drug	Structure	pKa	Melting Point (°C)	Molecular Weight (g/mol)	Maximum Wavelength (nm)
Diclofenac sodium		4.15	275–277	318.1	276

## 2. Materials and Methods

### 2.1. Preparation of MIL-88A Drug Carriers

MIL-88A materials were prepared using the hydro-/solvothermal method [1]. A mixture of fumaric acid (5 g, Sigma-Aldrich, Darmstadt, Germany,  $\geq 99.0\%$ ) and iron(III) chloride hexahydrate (3.21 g, Sigma-Aldrich, Darmstadt, Germany, 97%) was dissolved in 300 mL of solvent (distilled water or N,N-Dimethylformamide (DMF, Sigma-Aldrich, Darmstadt, Germany,  $\geq 99.8\%$ )). Then, the reaction mixture was transferred to Teflon-lined steel autoclaves and heated at varying temperatures (70 °C or 120 °C) for 24 h. Following cooling to room temperature, the precipitate was obtained via centrifugation at 6000 rpm for 10 min and washed with distilled water. Finally, the materials were dried overnight at 60 °C. Synthesized samples were denoted as MIL-88A-1 (H<sub>2</sub>O, 70 °C), MIL-88A-2 (H<sub>2</sub>O, 120 °C), MIL-88A-3 (DMF, 70 °C), and MIL-88A-4 (DMF, 120 °C).

### 2.2. Characterization of MIL-88A Carriers

#### 2.2.1. Powder X-ray Diffraction (XRD)

XRD analysis was carried out using a D8 Advance diffractometer (Bruker AXS, Karlsruhe, Germany) with Johansson monochromator (copper radiation  $K\alpha_1 = 1.5406 \text{ \AA}$ ) and silicon strip detector LynxEye. The measurements were performed in the  $2\theta$  range of 6–40° at room temperature with a step size of 0.01° and a scan rate of 0.05°/s in continuous mode.

#### 2.2.2. Scanning Electron Microscopy (SEM)

The morphology of MIL-88A materials was determined using a Quanta 250 FEG Scanning Electron Microscope (SEM) (FEI, Hillsboro, OR, USA). The analysis was carried

out under the following conditions: a working distance of 11.6 mm and an accelerating voltage of 10–15 kV. The samples were located on aluminum holders using carbon tape and coated with a 50 nm electrically conductive carbon layer. The experiment was performed in the secondary electron (SE) light.

### 2.2.3. Low-Temperature Nitrogen Sorption

To evaluate the textural characteristics of the MIL-88A materials, nitrogen adsorption/desorption was conducted at a low temperature of  $-196\text{ }^{\circ}\text{C}$  using the Quantachrome Autosorb IQ apparatus (Anton Paar GmbH, Graz, Austria). The Autosorb IQ apparatus allows for volumetric measurement of gas adsorption and desorption at relative pressure ranging from 0.001 to values slightly below 1.0. Before measurements, the MIL-88A materials were outgassed 12 h under vacuum at  $150\text{ }^{\circ}\text{C}$ . The Brunauer–Emmett–Teller (BET) method was used to calculate the specific surface areas of the samples, and the Barret–Joyner–Halenda (BJH) method was applied for pore size and volume assessment. The micropore surface area was determined using the t-plot method.

### 2.2.4. Thermogravimetric Analysis (TGA)

The MIL-88A samples' thermal stability was characterized using a Thermogravimetric Analyzer (TGA) Setsys 1200 (Setaram, Caluire, France). Measurements of the samples' stability (approximately 10 mg) were performed in airflow from ambient to  $1000\text{ }^{\circ}\text{C}$  at a constant rate of  $5\text{ }^{\circ}\text{C}/\text{min}$ . TGA analysis was conducted utilizing a sample pan made of platinum.

### 2.2.5. Fourier-Transform Infrared Spectroscopy (FT-IR)

The functional groups on the MIL-88A samples' surface before and after diclofenac sodium adsorption were analyzed by FT-IR spectroscopy. The measurements were carried out utilizing an FT-IR Bruker IFS66/S spectrometer (Bruker, Billerica, MA, USA) with the GLOBAR light source and Michelson interferometer. MIL-88A and MIL-88A—diclofenac sodium systems—were blended with anhydrous potassium bromide at a mass ratio of 1:200 mg and compressed to form a tablet. The analysis was conducted within a wavenumber range of  $4000\text{--}500\text{ cm}^{-1}$ .

## 2.3. Diclofenac Sodium Adsorption Studies

To examine the diclofenac sodium adsorption abilities of synthesized MIL-88A samples, a sequence of adsorption experiments was performed. Portions of 25 mg of each material were introduced into the drug solutions with a concentration range of 100–3000 mg/L. Next, the samples were continuously agitated for 2 h in the orbital shaker (KS 4000i control, IKA, Staufen, Germany) at a constant temperature ( $25 \pm 1\text{ }^{\circ}\text{C}$ ) and shaking rate of 250 rpm. The residual concentration of the drug solution was determined by an Agilent Cary 60 UV-Vis spectrophotometer (Santa Clara, CA, USA) at a wavelength of 276 nm. The sorption capacities ( $Q_e$ ) of the MIL-88A were calculated using the following formula:

$$Q_e = \frac{C_0 - C_e}{m} \quad (1)$$

To describe the MIL-88A carrier-diclofenac sodium interactions, the adsorption data were fitted to non-linear Langmuir and Freundlich adsorption models. The determination of the adsorption mechanism was based on the correlation coefficients ( $R^2$ ) of the models.

The non-linear Langmuir isotherm is described by Equation (2):

$$Q_e = Q_m K_L \frac{C_e}{1 + K_L C_e} \quad (2)$$

where  $Q_m$  is the maximum adsorption capacity (mg/g), and the  $K_L$  constant is associated with the free energy of adsorption (L/mg).

The non-linear form of Freundlich isotherm can be expressed by Equation (3):

$$Q_e = K_F \cdot C_e^{1/n} \quad (3)$$

where  $n$  is the constant representing the degree of favorability of the adsorption process, and  $K_F$  is related to the adsorption affinity of the adsorbent.

#### 2.4. Diclofenac Sodium Release Studies

The in vitro release of the drug from the synthesized MIL-88A materials was conducted using cellulose dialysis tubing (Sigma-Aldrich, Darmstadt, Germany). Before the liberation process, 25 mg of MIL-88A materials were added into the diclofenac solution (5 mg of DS in 3 mL aqueous solution) and agitated for 2 h. In the next step, the solution was evaporated overnight in an oven set at 60 °C. The release studies were performed in a phosphate buffer of pH 6.8, representing intestinal conditions and maintained at 37.0 °C ± 0.5 °C. The system was stirred at a speed of 200 rpm. In order to prepare the dissolution medium, 100 mL of 0.1 M KH<sub>2</sub>PO<sub>4</sub> was mixed with 44.8 mL of 0.1 M NaOH and 55.2 mL of distilled water. At the interval of 15 min in the first 3 h and 30 min in the next 2 h, 3 mL of the mixture was collected, and the amount of released diclofenac sodium was assessed using a UV–Vis spectrophotometer at  $\lambda = 276$  nm. Measurements were also conducted for the interval of 24 h and 42 h. Subsequently, the cumulative percentage of the released drug was calculated. The liberation results were correlated to five mathematical models to describe the release mechanism: zero-order (% DS release vs. time; Equation (4)), first-order (log of % DS release vs. time; Equation (5)), Higuchi's model (% DS release vs. square root of time; Equation (6)), Hixson–Crowell (cube root of % DS remaining vs. time; Equation (7)), and Korsmeyer–Peppas model (log of % DS vs. log time; Equation (8)) [41]. Experimental data were analyzed using OriginPro 2023 [42].

$$F_t = k_0 t_e \quad (4)$$

$$F_t = 1 - e^{-kt} \quad (5)$$

$$F_t = k_H \sqrt{t} \quad (6)$$

$$\sqrt[3]{F_0} - \sqrt[3]{F_t} = k_{HC} t \quad (7)$$

$$F_t = kt^n \quad (8)$$

$F_t$  is the fraction of diclofenac sodium release in time;  $F_0$  represents the initial quantity of diclofenac sodium incorporated into the nanocarrier  $k_0$ ,  $k_t$ ,  $k_H$ ,  $k_{HC}$  and  $k$  are the release constants of particular kinetic models; and  $n$  is the diffusion exponent.

### 3. Results and Discussion

#### 3.1. Physicochemical Characterization of MIL-88A Carriers

The XRD patterns of the synthesized materials are shown in Figure 1. They confirmed obtaining crystalline phases specific to MIL-88A metal-organic frameworks. Depending on the synthesis temperature and solvent used, the characteristic reflections registered for all materials have slightly different positions, widths, and intensities in comparison to simulated patterns. This is consistent with previous literature reports [26,43]. Additionally, changes could be attributed to the presence of free fumaric acid or water molecules in the material pores [26]. In the case of MIL-88A-1 and MIL-88A-2 samples, prepared in distilled water, the most intensive reflections located at 2θ~10.8°, 11.8° and 10.1°, 10.8°, respectively, can be assigned to the (100) and (101) planes. When DMF was used as a solvent during synthesis, there was a transition in the crystal orientation of MIL-88A from (101) to (100). The XRD patterns of MIL-88A-3 and MIL-88A-4 contain distinct reflections at 2θ~10.1°, 10.8° and 10.8°, 11.8°, respectively. Slight shifts of diffraction peaks indicate the flexibility of the MIL-88A structure [44].

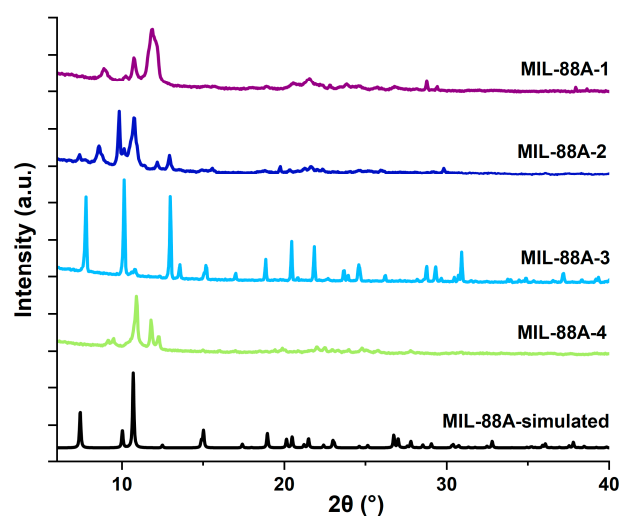


**Figure 1.** XRD patterns of materials obtained in the high-angle range.

Physisorption of nitrogen was conducted for all the iron-based MOF carriers, and the resulting isotherms are illustrated in Figure 2. The nitrogen adsorption/desorption isotherm of MIL-88A-1, prepared in distilled water at 70 °C, has a shape comparable to type IV in line with the IUPAC (International Union of Pure and Applied Chemistry) classification, specific to mesoporous materials [26]. In turn, the MIL-88A-2 sample synthesized at a higher temperature (120 °C) exhibits a type I nitrogen adsorption/desorption curve, indicating the presence of micropores in its structure. For this isotherm, a stage of rapid growth is observed at low relative pressure values, followed by saturation [45]. The nitrogen adsorption/desorption curves of the MIL-88A-3 and MIL-88A-4 materials obtained in *N,N*-Dimethylformamide correspond to the combination of I and II types [26]. They have a microporous structure with a small amount of macropores. The textural parameters of MIL-88A materials are summarized in Table 2. MIL-88A-1 was characterized by the lowest specific surface area and total pore volume—10 m<sup>2</sup>/g and 0.05 cm<sup>3</sup>/g, respectively. These values correspond to the results reported in the literature for MIL-88A synthesized under similar conditions [43,46,47]. Synthesis of MIL-88A-2 material at a higher temperature leads to the generation of higher porosity. It shows a higher specific surface area of 292 m<sup>2</sup>/g, a pore volume of 0.21 cm<sup>3</sup>/g, and an average pore diameter of 2.83 nm. MIL-88A-2 micropore surface area represents 89% of the total surface area, confirming mainly the microporous character of this material. The best-developed specific surface areas were obtained for MIL-88A-3 and MIL-88A-4 materials synthesized in *N,N*-Dimethylformamide, 326 and 307 m<sup>2</sup>/g, respectively, with the micropore surface areas of 279 and 122 m<sup>2</sup>/g. The difference between the specific surface area and pore volume of MIL-88A-1 and other samples could be ascribed to the framework opening and closing [48]. This phenomenon is characterized by a reversible cell volume doubling during the conversion of topology from closed to open [49].

**Table 2.** Textural parameters of MIL-88A carriers.

Sample	BET Surface Area (m <sup>2</sup> /g)	Total Pore Volume (cm <sup>3</sup> /g)	Average Pore Diameter (nm)	Micropore Area (m <sup>2</sup> /g)
MIL-88A-1	10	0.05	20.30	-
MIL-88A-2	292	0.21	2.83	261
MIL-88A-3	326	0.47	5.74	279
MIL-88A-4	307	0.33	4.27	122

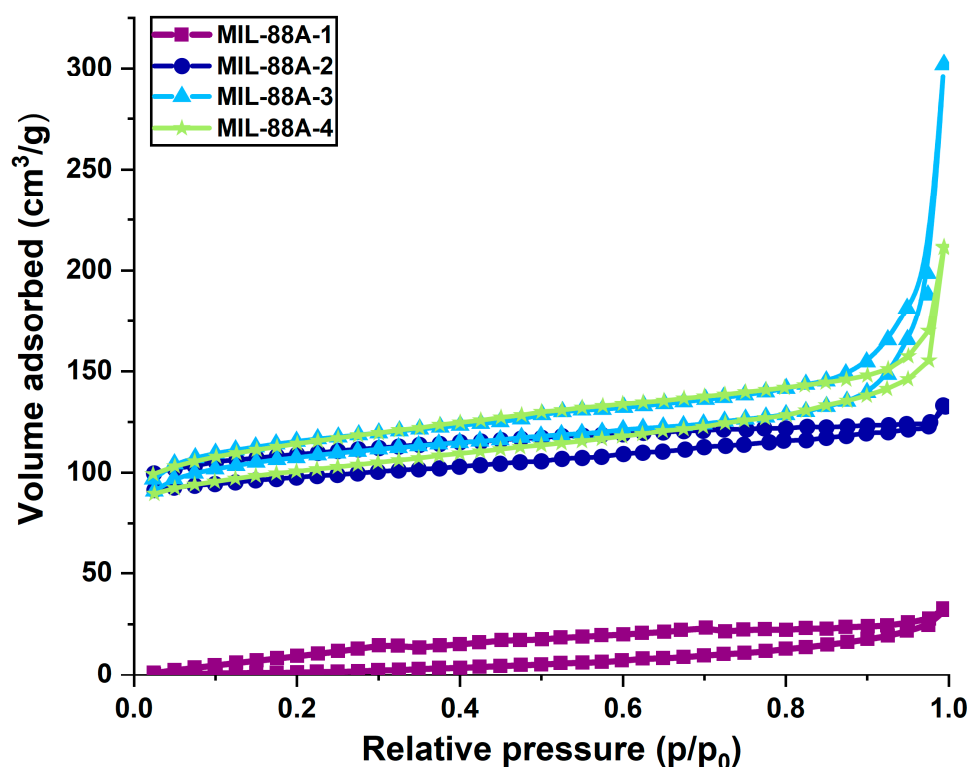
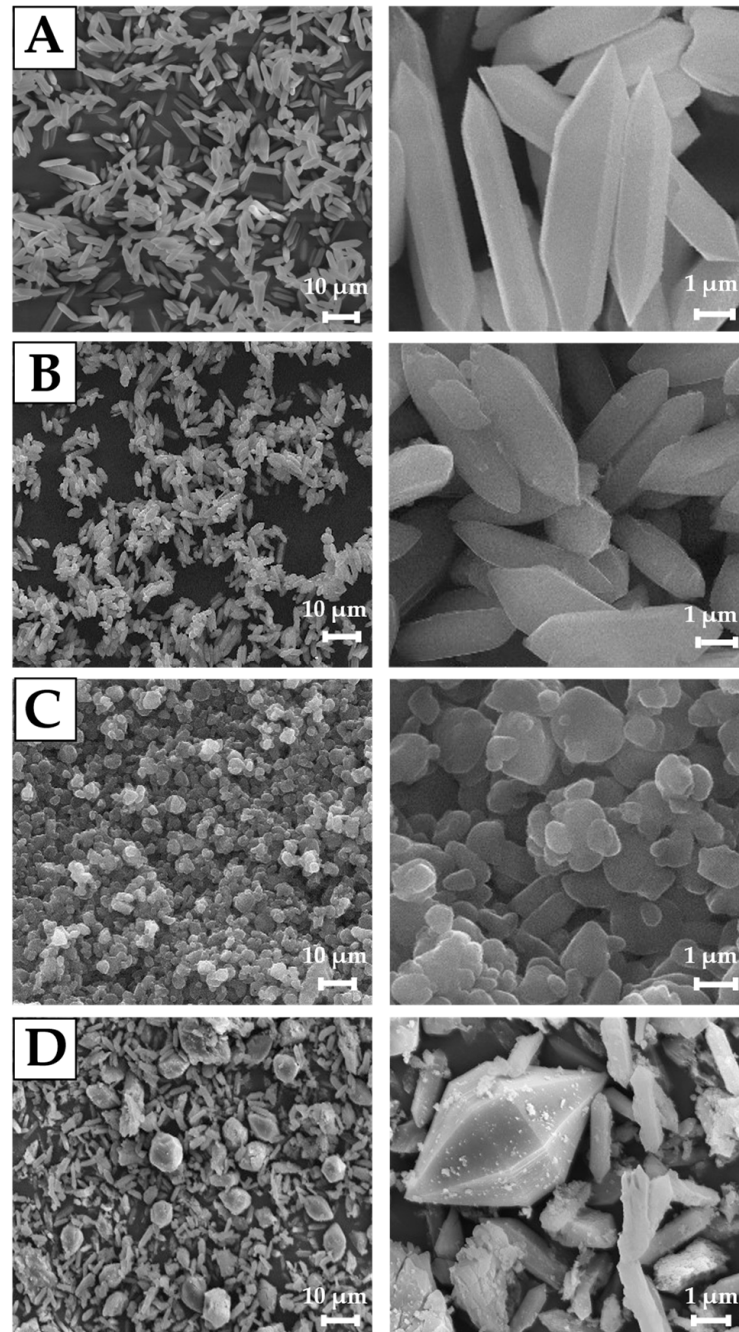


Figure 2. N<sub>2</sub> adsorption/desorption isotherms of MIL-88A materials.

Scanning electron microscopy (SEM) images demonstrate that the MIL-88A materials with different morphologies were successfully prepared using the hydro-/solvothermal method. The particle size is strongly influenced by the value of the dipole moment of solvents due to the changes in linker solubility, solvent–nanoparticle interface, and superficial tension [50]. It is observed that after synthesis in distilled water at 70 °C, the MIL-88A-1 sample presents a hexagonal rod-like morphology with an average length of 7.5 μm (Figure 3A) [51]. Upon increasing the synthesis temperature, the mean particle size of MIL-88A-2 decreases to approximately 5.5 μm, but also the surface roughness is visible (Figure 3B). The morphology of MIL-88A-3 prepared in DMF at 70 °C changed to a spherical (Figure 3C). DMF retards the crystallization rate of MOF by effectively solvating Fe(III) ions in the organic medium, which could result in lower particle agglomeration and stop rod-like crystallite formation [45,52]. The particle size of this sample is much smaller compared to the materials prepared in distilled water: about 500 nm. These size differences are associated with higher dipole moment of DMF than water (3.86 D and 1.856 D, respectively) and greater linker solubility in DMF than in water [53]. It could result in faster nucleation rates, leading to smaller crystal sizes [54]. The converse phenomenon is evident in the case of the MIL-88A-4 sample (Figure 3D). Implementation of the same solvent (DMF) but a higher temperature (120 °C) caused the formation of crystals with two different shapes—rods and diamonds, the most common for materials synthesized in DMF. It was observed that the size of diamond-like particles was about 13 μm and rod-like—2 μm in length.

The thermal stability of the MIL-88A samples was evaluated via TG analysis (Figure 4). The initial weight loss, occurring below 100 °C, is associated with the evaporation of moisture [55]. For MIL-88A-1 and MIL-88A-2, the further mass loss observed at 300 and 298 °C, respectively, is attributed to fumaric acid degradation, which proves that it is inherent in the MIL-88A structure [56]. The mass loss noted in the temperature range of 360–440 °C is related to the collapse of the metal-organic skeleton [57,58]. The third stage visible on the TG curve of MIL-88A-1 at 646 °C can be associated with the iron oxide conformation or the conversion between iron oxides [59]. Weight loss of MIL-88A-1

and MIL-88A-2 was 69 and 55%, respectively. In turn, for MIL-88A-3 and MIL-88A-4, weight loss associated with linker decomposition occurred to a greater extent at lower temperatures: 283 and 287 °C. After this step, the weight of MIL-88A-3 and MIL-88A-4 samples is almost unchanged until 1000 °C. The samples synthesized in distilled water (MIL-88A-1 and MIL-88A-2) are slightly more thermally stable than materials synthesized in DMF.



**Figure 3.** SEM images of: (A) MIL-88A-1, (B) MIL-88A-2, (C) MIL-88A-3, (D) MIL-88A-4 carriers.

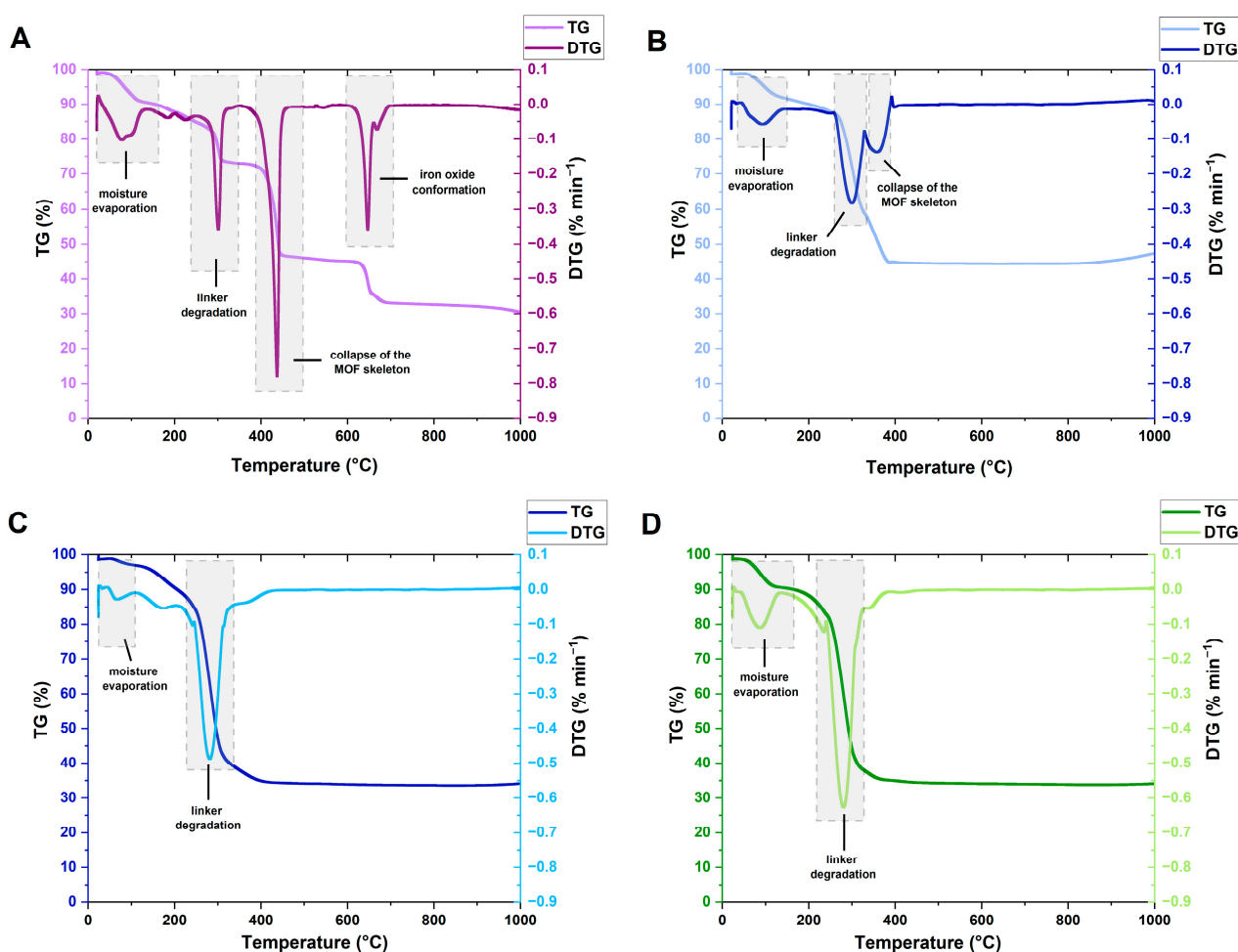


**Figure 4.** TG and DTG curves of (A)—MIL-88A-1; (B)—MIL-88A-2; (C)—MIL-88A-3; (D)—MIL-88A-4.

### 3.2. Adsorption and Release of Diclofenac Sodium

All synthesized under different conditions, MIL-88A materials were applied as diclofenac sodium carriers. To evaluate the efficacy of the drug adsorption process on the sample surfaces, the FT-IR spectra were recorded (Figure 5A–D). Regarding the pristine MIL-88A samples, the absorption band in the wavenumber range of 3200–3600  $\text{cm}^{-1}$  is associated with hydroxyl groups in the structure or adsorbed moisture. The bands at  $\sim 1604$  and  $\sim 1400$   $\text{cm}^{-1}$  could be attributed to the symmetric and asymmetric vibrations of the fumarate ligand C=O groups [60,61]. In turn, at around 1215 and 983  $\text{cm}^{-1}$ , the absorption bands originating from the vibration mode of C-O in carboxylic groups and C-H were detected. The band at 640  $\text{cm}^{-1}$  could be associated with the presence of the carbonyl group. In addition, the absorption band at  $\sim 556$   $\text{cm}^{-1}$  can be ascribed to the Fe-O stretching vibrations [61–63]. The presence of the mentioned absorption bands signifies the successful coordination of fumaric acid and iron ions in the MIL-88A structure [64–66]. The FT-IR spectrum of diclofenac sodium contains distinct bands at 3390  $\text{cm}^{-1}$ , 1574  $\text{cm}^{-1}$ , 1289  $\text{cm}^{-1}$ , and 746  $\text{cm}^{-1}$  related to the N-H groups of the secondary amine, C=O from carboxyl ions, and C-CO-C, as well as C-Cl vibrations, respectively (Figure 5E) [67]. The drug-loaded MIL-88A samples spectra revealed the band at approximately 3320  $\text{cm}^{-1}$  which could be associated with the N-H stretching vibrations of the secondary amine from diclofenac sodium. Moreover, the bands at wavenumbers around 1580  $\text{cm}^{-1}$  and 1450  $\text{cm}^{-1}$ , attributed in the literature to C=O and C=C stretching vibrations, are noted [67–69]. The materials show a new band at 1290  $\text{cm}^{-1}$  from the C-CO-C bond, confirming the presence of the drug on the sample surfaces [70]. The band at 766  $\text{cm}^{-1}$  can be related to the stretching vibrations of

C-Cl. The existence of these absorption bands validated the successful adsorption of the drug on the surface of all MIL-88A materials.

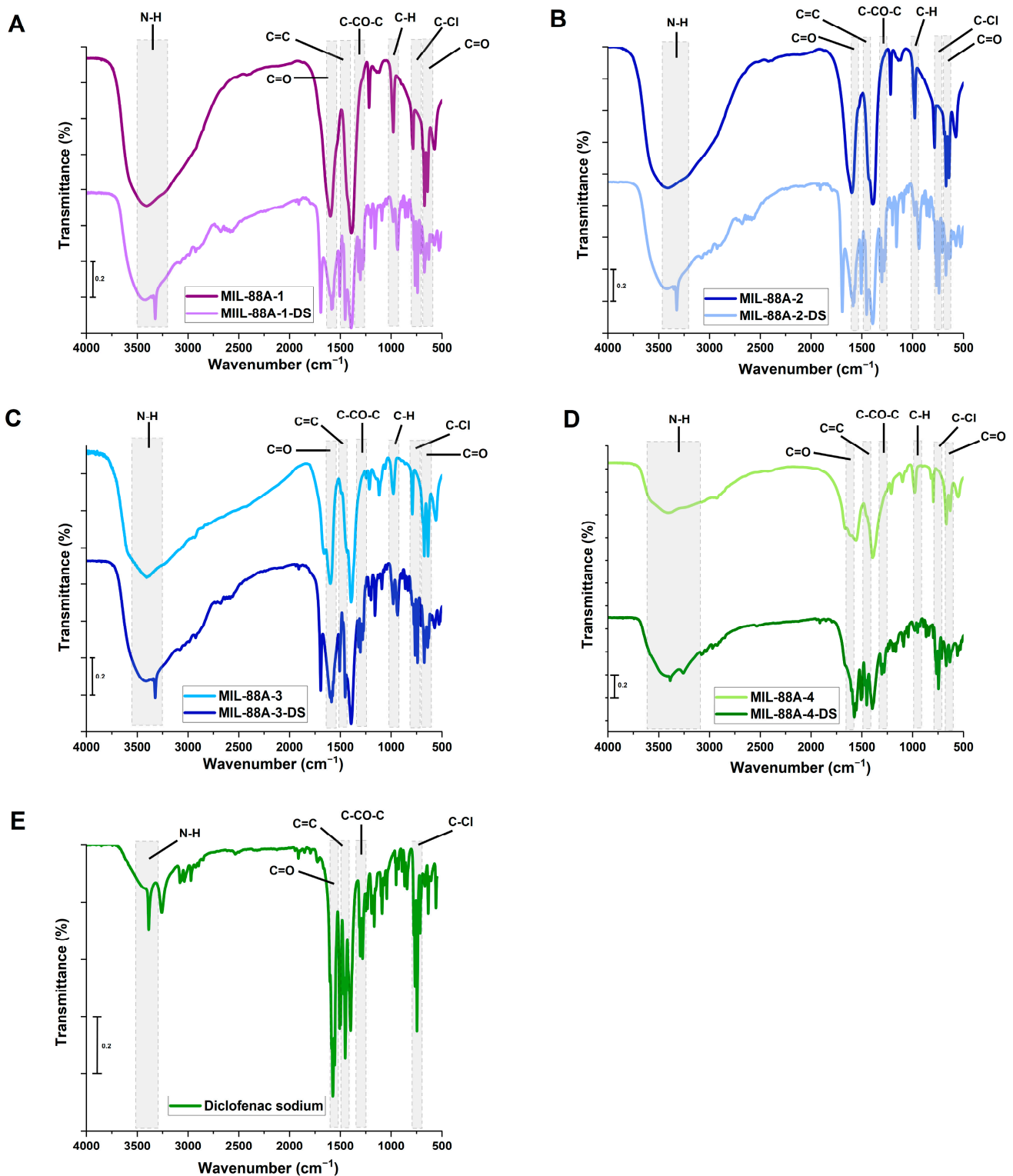


**Figure 5.** FT-IR spectra of (A)—MIL-88A-1; (B)—MIL-88A-2; (C)—MIL-88A-3; (D)—MIL-88A-4 samples before and after drug adsorption, and (E)—diclofenac sodium.

Figure 6 depicts the equilibrium adsorption isotherms of diclofenac sodium onto metal-organic frameworks. It was noted that the quantity of adsorbed drug significantly

increased with increasing initial concentration of its solution until reaching the saturation point of adsorption. At low initial drug concentrations, the active sites of samples were highly accessible for diclofenac sodium, and its adsorption was random. At the higher drug solution concentrations, the sorption capacity was constant because all available active sites were occupied by either drug or water molecules [71]. The lowest sorption capacity toward diclofenac sodium exhibits samples synthesized in DMF: MIL-88A-3 and MIL-88A-4 (833 mg/g and 1244 mg/g, respectively). The most effective adsorbents of the drug are MIL-88A-1 (2021 mg/g) and MIL-88A-2 (1500 mg/g) prepared in distilled water, although they have a smaller specific surface area and pore volume than samples synthesized in DMF. This phenomenon could be associated with the structural flexibility of MIL-88A affected by the adsorption of polar solvent molecules [72]. Materials synthesized in distilled water are more flexible owing to the presence of hydrogen bonds between water (guest molecules) and the framework [73–75]. The structural flexibility of these MOFs allows them to accommodate drug molecules of different sizes [76]. Based on the aforementioned results, the drug adsorption process engaged structural parameters and interactions between the samples and drug molecules. One of the primary factors influencing adsorption is the pore size of porous adsorbents. The average pore diameters of the MIL-88A materials, in the range of 2.83–20.3 nm, were higher than the molecular dimensions of the diclofenac sodium (0.97 nm × 0.71 nm × 0.47 nm). The adsorption process was enhanced by allowing unrestricted drug transport within the pores, as steric obstacles do not impose limitations [77]. Taking into account the morphology of the synthesized materials, it can be observed that rod-like particles significantly increase the amount of adsorbed drug. High MIL-88A/drug affinity was also the result of unique interactions between diclofenac sodium and samples. The adsorption of drugs onto the surface of MIL-88A samples is primarily based on hydrogen bonding, facilitated by the presence of proton donors and acceptors in both the drug and the samples. The amine groups in diclofenac sodium could act as proton donors, and the electronegative parts of materials as proton acceptors. On the other side, the formation of hydrogen bonds may occur between  $\mu_3\text{-OH}([\text{Fe}(\text{OH})])$  in MIL-88A and functional groups containing oxygen or nitrogen in the diclofenac sodium molecules [26,78]. Secondly, the metal coordination effect enhances the effective adsorption of drug molecules via the interaction between the MIL-88A central iron trimers and the nitrogen and oxygen functional groups of the drug [57,76]. Finally, in addition to these two types of interplays, electrostatic interactions may affect the adsorption of diclofenac onto the MIL-88A samples. The isoelectric point of MIL-88A is 6.0, and the pKa value for diclofenac sodium is 4.0 [79,80]. This means that the samples maintain a positive surface charge until the pH reaches 6, while diclofenac sodium takes on an anionic form when the pH exceeds 4 (Figure 7). The pH of the drug solution was 5.5; hence, the drug adsorption at this pH value can be based on the electrostatic interactions occurring between the anions of diclofenac sodium and the positively charged surface of MIL-88A [57]. The possible mechanism of drug adsorption onto MIL-88A materials is depicted in Figure 8. Table 3 compares the maximum sorption capacity of the MIL-88A-1 sample synthesized in distilled water at lower temperatures with other adsorbents described in the literature. The MIL-88A-1 material adsorbed the highest amount of diclofenac sodium. In contrast to other MOF materials prepared in DMF (i.e., UIO-66, MOR-1, MIL-100,  $[\text{Cu}(\text{BTTA})]_n \cdot 2\text{DMF}$ ), synthesis of MIL-88A-1 conducted in distilled water under mild conditions makes it more environmentally friendly. The high adsorption ability of MIL-88A-1 can be attributed to its flexible structure and breathing effect, as well as different types of interactions with diclofenac sodium: hydrogen bonding, metal coordination, and electrostatic interactions.

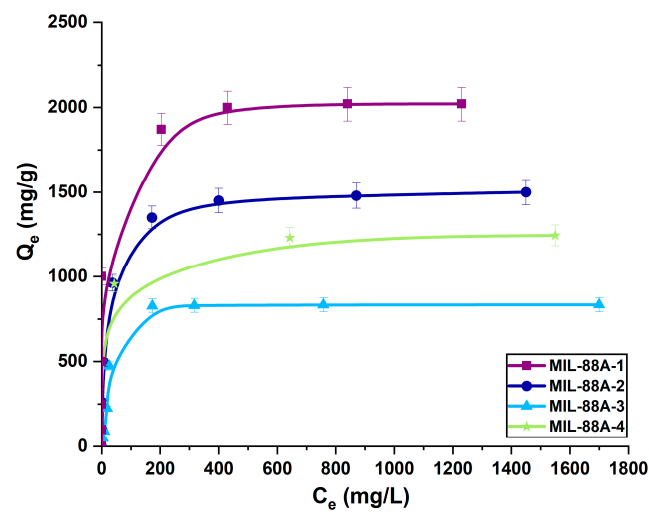


Figure 6. Adsorption isotherms of diclofenac sodium on the surface of MIL-88A carriers.

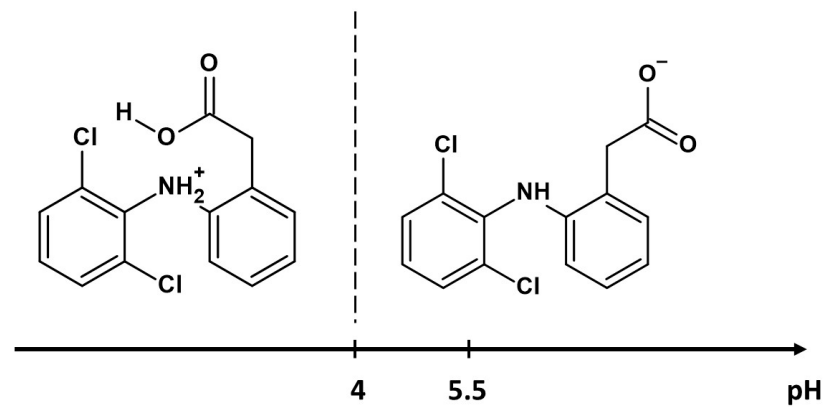


Figure 7. Different forms of diclofenac sodium at various pH conditions.

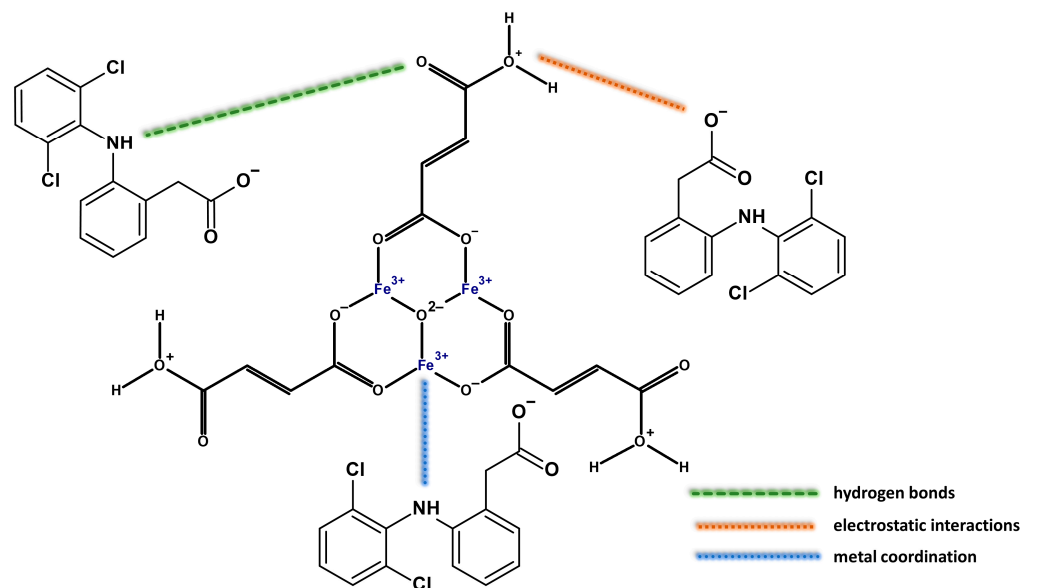
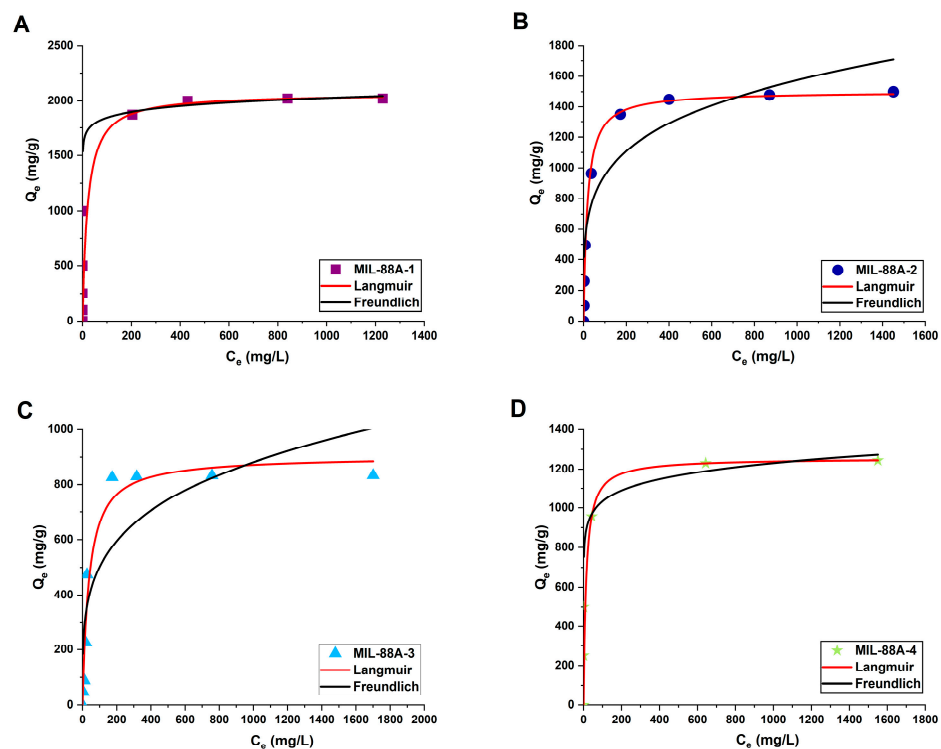


Figure 8. Proposed mechanism of the interactions between diclofenac sodium and MIL-88A samples.

**Table 3.** Comparison of the performance of various materials in diclofenac sodium adsorption.

Material	Material Type	Specific Surface Area (m <sup>2</sup> /g)	Maximum Sorption Capacities (mg/g)	Ref.
Pyridine functionalized mesoporous silica	silica	322	352	
Thiol functionalized mesoporous silica	silica	493	48	[81]
Amine functionalized mesoporous silica	silica	358	328	
Al <sub>2</sub> O <sub>3</sub> /La <sub>2</sub> O <sub>3</sub>	aluminum oxide	156	82	[82]
F-300	carbon	847	108	[83]
PC-1000	carbon	1236	392	[84]
Alginate/carbon films	carbon composite	35	30	[85]
UiO-66-(COOFe) <sub>2</sub>	Zr-based MOF	684	860	[86]
MOF-525	Zr-based MOF	1955	792	[87]
MOF-808	Zr-based MOF	1517	830	[88]
UiO-66/MWCNT	Zr-based MOF composite	-	256	[89]
MOR-1	Zr-based MOF	1097	315	[90]
RT-iCOF	ionic covalent organic framework	69	875	[91]
MCOF-2	magnetic covalent organic frameworks	335	565	[92]
[Cu(BTTA)] <sub>n</sub> ·2DMF	Cu-based MOF	-	650	[93]
ZIF-8-NPs	Zn-based MOF	1568	843	[94]
Fe <sub>3</sub> O <sub>4</sub> @MIL-100(Fe)	Fe-based MOF	1245	400	[95]
MIL-100	Fe-based MOF	1235	773	[96]
12%PTA@MIL101(Cr)	Cr-based MOF composite	1909	413	[97]
MIL-88A-1	Fe-based MOF	10	2021	this work

To understand the adsorption mechanism, diclofenac sodium adsorption isotherms were fitted to the non-linear form of Langmuir and Freundlich models (Figure 9). It was found that the correlation coefficients  $R^2$  for the Freundlich model are higher than for Langmuir in the case of drug adsorption onto MIL-88A-1 (distilled water, 70 °C) and MIL-88A-4 (DMF, 120 °C) (Table 4). It implies multilayer adsorption, which assumes the interaction between adsorbed molecules on a non-uniform surface [26]. The calculations indicate that the Langmuir model can best represent the adsorption of diclofenac sodium onto MIL-88A-2 (distilled water, 120 °C) and MIL-88A-3 (DMF, 70 °C) (Table 4). It suggests that drug molecules form a monolayer on the surface of the MIL-88A materials, and the adsorption process is mainly controlled by host–guest interactions [93,98]. There is no lateral interaction between the adsorbed drug molecules [99]. The  $K_L$  constant values for all samples indicate that the bonding between diclofenac sodium and MIL-88A-4 is the strongest [100]. The value of  $1/n$  determined from the Freundlich isotherm was less than 1 for all samples, confirming that the adsorption of diclofenac sodium is thermodynamically favorable [18]. The maximum theoretical values ( $Q_{max}$ ) of materials' adsorption capacities toward diclofenac sodium are comparable to those obtained experimentally.



**Figure 9.** Non-linear fitting of diclofenac sodium adsorption isotherms to Langmuir and Freundlich models for (A) MIL-88A-1, (B) MIL-88A-2, (C) MIL-88A-3, (D) MIL-88A-4.

**Table 4.** The parameters of non-linear Langmuir and Freundlich isotherm models fitted to equilibrium data of diclofenac sodium adsorption on the surface of MIL-88A samples.

Material	Langmuir			Freundlich		
	$Q_{\max}$	$K_L$	$R^2$	$K_F$	$1/n$	$R^2$
MIL-88A-1	2070	0.049	0.793	1523	0.04	0.798
MIL-88A-2	1502	0.058	0.995	349	0.22	0.867
MIL-88A-3	905	0.027	0.967	162	0.25	0.758
MIL-88A-4	1255	0.075	0.773	728	0.08	0.951

The release studies of diclofenac sodium from MIL-88A materials were performed in a phosphate buffer of pH 6.8, simulating intestinal fluid. The release profiles of the drug from MIL-88A carriers are shown in Figure 10. The percentage of the drug desorbed from the metal-organic frameworks ranges from 58 to 97%, depending on their synthesis conditions. Considering that the molecular size of diclofenac sodium is  $0.97 \text{ nm} \times 0.71 \text{ nm} \times 0.47 \text{ nm}$ , it should be assumed that the drug diffusion rate is affected by samples' textural parameters and functional groups present on the surface [77,101]. The drug release profiles obtained for MIL-88A-1, MIL-88A-2, and MIL-88A-3 materials showed a two-stage diffusion process. It indicates diclofenac sodium rapid release during the initial stage of the experiment due to the presence of its molecules mainly on the carriers' external surface, followed by a subsequent stage of slower release of the drug from the pores over an extended period [102]. At pH 6.8, which simulated intestinal condition, the highest drug amount was liberated from rod-like MIL-88A-1, synthesized in water at  $70^\circ \text{C}$ . The release profile of the diclofenac sodium from the sample presented a high burst liberation of the drug (70%) during the first six hours and then slower desorption of 27% after 30 h. This material was characterized by the largest pore diameter, which resulted in weaker interactions between material pore walls and diclofenac sodium molecules. The extended drug release from the MIL-88A-2 sample in simulated intestinal fluid finished within 32 h. Regarding MIL-88A-2, MIL-88A-3, and MIL-88A-4 materials, larger specific surface area and porosity

promote higher accessibility of adsorption sites, leading to stronger interactions between the drug molecules and the materials' surface [103]. Drug desorption from MIL-88A-3 and MIL-88A-4 reached about 58% after 30 h, extending the therapeutic effect of this drug in the human body. The high percentage of drug release (from 58% for samples synthesized in DMF to 97% for material obtained in water at 70 °C) at pH 6.8 could be associated with the repulsion between the drug's anionic form and the negatively charged surface of carriers [104–106].

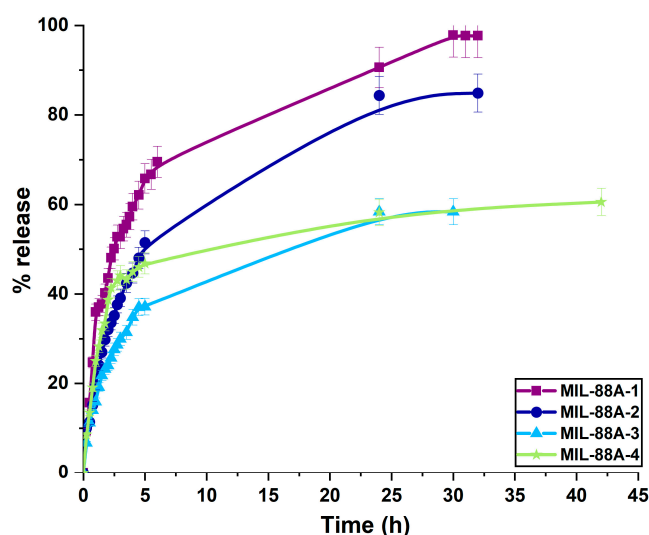


**Figure 10.** Diclofenac sodium release profiles for MIL-88A carriers at pH 6.8.

Various materials have been presented in the literature as advanced diclofenac sodium delivery systems. Zauska and co-workers [107] utilized SBA-15 silica functionalized with polyethyleneimine polymers as a drug carrier. Experimental results showed that at pH 7.4 and 37 °C, simulating the small intestine environment, the SBA-15(C) sample released 89.4% of diclofenac sodium. Nikolova et al. [108] applied chitosan and sodium alginate polyelectrolyte complexes for controlled DS liberation at pH 6.8. They reported a linear drug release profile in the first 6 h. Vargas and co-workers [109] evaluated surfactant-modified clinoptilolite and chabazite as platforms for diclofenac sodium delivery. It was shown that clinoptilolite causes an immediate liberation of the drug within 1 h (57%) followed by incremental release during the next 5 h (about 85%) at pH 7.4. Lucena et al. [110] synthesized BioMOF-Zn (Zn(II) coordination polymer with 4,4'-biphenyl-dicarboxylic acid (BPDC) and adenine linker) as a diclofenac sodium delivery platform. Approximately 56% of the drug was desorbed from the sample at pH 7.4. The results obtained in the case of functionalized SBA-15 silica, as well as chitosan and sodium alginate polyelectrolyte complexes, are comparable to the release of diclofenac sodium from MIL-88A-1 and MIL-88A-2 materials. In turn, MIL-88A-3 and Zn-based BioMOF were characterized by similar release capabilities. The components of MIL-88A (iron ions and fumaric acid) render it a biocompatible and non-toxic drug carrier.

Different kinetic models (zero-order, first-order, Korsmeyer–Peppas, Hixson–Crowell, and Higuchi) were fitted to the experimental data to determine the diclofenac sodium release rate and mechanism. To assess the diffusion kinetics, kinetic values of release constants ( $k$ ), release exponent ( $n$ ), and correlation coefficient ( $R^2$ ) were estimated and summarized in Table 5. The release profile of the drug from MIL-88A-1 prepared in distilled water at a lower temperature is best fitted to the first-order kinetic model, which is common for a drug release from porous carriers. It is a concentration-dependent drug release mechanism [111]. It implies that the diclofenac sodium release rate diminishes as the concentration gradient of the drug decreases over time [112]. The highest values of  $R^2$  were noted for the Higuchi model in the case of MIL-88A-2, MIL-88A-3, and MIL-88A-4, which

describes the amount of drug liberated as a function of the square root of time [113]. It is characteristic of the drug release from an insoluble matrix [114].

**Table 5.** Kinetic release parameters describing the mechanism of diclofenac sodium diffusion from MIL-88A materials.

Sample	Zero-Order		First-Order		Higuchi		Hixson–Crowell		Korsmeyer–Peppas		
	$k_0$	$R^2$	$k_1$	$R^2$	$k_H$	$R^2$	$k_{HC}$	$R^2$	$k_{KP}$	$n$	$R^2$
MIL-88A-1	7.077	0.973	0.154	0.992	24.778	0.990	0.183	0.988	33.787	0.403	0.984
MIL-88A-2	8.372	0.952	0.127	0.982	25.649	0.993	0.171	0.974	19.458	0.637	0.984
MIL-88A-3	6.647	0.954	0.087	0.974	18.307	0.996	0.123	0.968	16.592	0.540	0.995
MIL-88A-4	13.035	0.940	0.185	0.964	30.678	0.986	0.254	0.957	23.319	0.66	0.976

#### 4. Conclusions

In summary, the series of MIL-88A metal-organic frameworks were prepared under different conditions: temperature (70 and 120 °C) and solvent (distilled water and DMF). It was found that synthesis factors strongly influence materials' physicochemical properties and sorption abilities. The highest surface area and pore volume exhibited MIL-88A-3 synthesized in DMF at a lower temperature, while the smallest textural parameters, MIL-88A-1, prepared in distilled water at 70 °C. The materials synthesized in water (MIL-88A-1 and MIL-88A-2) were more thermally stable than samples obtained in DMF. MIL-88A-1 and MIL-88A-2 samples indicated rod-like morphology, while MIL-88A-3 and MIL-88A-4 particles were characterized by spherical or diamond shapes, respectively. Diclofenac sodium adsorption onto metal-organic framework surfaces occurred mainly via hydrogen bonding and metal coordination, as well as electrostatic interactions. The highest amount of drug was adsorbed onto MIL-88A-1 (2021 mg/g) with the smallest specific surface area and pore volume, which implies, that the adsorption course is mainly influenced by the surface moieties. The drug was desorbed from the MIL-88A carriers to a phosphate buffer of pH 6.8 in two stages. At first, the drug was released quickly from the outer surface of MIL-88A materials, followed by a gradual and controlled diffusion of its molecules from inside the pores. The outcomes of this study confirm the potential of MIL-88A carriers to be used as drug delivery platforms in anti-migraine therapy.

**Author Contributions:** A.G.—Investigation, Visualization, Data curation, Writing—Original Draft Preparation; J.G.—Conceptualization, Supervision, Methodology, Writing—Review and Editing. All authors have read and agreed to the published version of the manuscript.

**Funding:** This research received no external funding.

**Institutional Review Board Statement:** Not applicable.

**Informed Consent Statement:** Not applicable.

**Data Availability Statement:** The data presented in this study are available on request from the corresponding author. The data are not publicly available due to privacy reasons.

**Conflicts of Interest:** The authors declare no conflict of interest.

#### References

- Steiner, T.J.; Stovner, L.J. Global Epidemiology of Migraine and Its Implications for Public Health and Health Policy. *Nat. Rev. Neurol.* **2023**, *19*, 109–117. [[CrossRef](#)] [[PubMed](#)]
- Chalmer, M.A.; Kogelman, L.J.A.; Callesen, I.; Christensen, C.G.; Techlo, T.R.; Møller, P.L.; Davidsson, O.B.; Olofsson, I.A.; Schwinn, M.; Mikkelsen, S.; et al. Sex Differences in Clinical Characteristics of Migraine and Its Burden: A Population-Based Study. *Eur. J. Neurol.* **2023**, *30*, 1774–1784. [[CrossRef](#)] [[PubMed](#)]
- Rossi, M.F.; Tumminello, A.; Marconi, M.; Gualano, M.R.; Santoro, P.E.; Malorni, W.; Moscato, U. Sex and Gender Differences in Migraines: A Narrative Review. *Neurol. Sci.* **2022**, *43*, 5729–5734. [[CrossRef](#)] [[PubMed](#)]
- Ahmad, S.R.; Rosendale, N. Sex and Gender Considerations in Episodic Migraine. *Curr. Pain Headache Rep.* **2022**, *26*, 505–516. [[CrossRef](#)] [[PubMed](#)]

5. Robbins, M.S. Diagnosis and Management of Headache: A Review. *JAMA—J. Am. Med. Assoc.* **2021**, *325*, 1874–1885. [[CrossRef](#)] [[PubMed](#)]
6. Noor, N.; Lachute, C.; Root, M.; Rogers, J.; Richard, M.; Varrassi, G.; Urits, I.; Viswanath, O.; Khater, N.; Kaye, A.D. A Comprehensive Review of Celecoxib Oral Solution for the Acute Treatment of Migraine. *Health Psychol. Res.* **2022**, *10*, 34265. [[CrossRef](#)] [[PubMed](#)]
7. Rist, P.M.; Buring, J.E.; Cook, N.R.; Kurth, T. Contribution of Migraine to Cardiovascular Disease Risk Prediction. *J. Am. Coll. Cardiol.* **2023**, *81*, 2246–2254. [[CrossRef](#)]
8. Geppetti, P.; De Cesaris, F.; Benemei, S.; Cortelli, P.; Cevoli, S.; Pierangeli, G.; Favoni, V.; Lisotto, C.; Usai, S.; Frediani, F.; et al. Self-Administered Subcutaneous Diclofenac Sodium in Acute Migraine Attack: A Randomized, Double-Blind, Placebo-Controlled Dose-Finding Pilot Study. *Cephalalgia* **2022**, *42*, 1058–1070. [[CrossRef](#)]
9. Sohail, R.; Mathew, M.; Patel, K.K.; Reddy, S.A.; Haider, Z.; Naria, M.; Habib, A.; Abdin, Z.U.; Razzaq Chaudhry, W.; Akbar, A. Effects of Non-Steroidal Anti-Inflammatory Drugs (NSAIDs) and Gastroprotective NSAIDs on the Gastrointestinal Tract: A Narrative Review. *Cureus* **2023**, *15*, e37080. [[CrossRef](#)]
10. Singh, A.P.; Biswas, A.; Shukla, A.; Maiti, P. Targeted Therapy in Chronic Diseases Using Nanomaterial-Based Drug Delivery Vehicles. *Signal Transduct. Target. Ther.* **2019**, *4*, 33. [[CrossRef](#)]
11. Dang, Y.; Guan, J. Nanoparticle-Based Drug Delivery Systems for Cancer Therapy. *Smart Mater. Med.* **2020**, *1*, 10–19. [[CrossRef](#)] [[PubMed](#)]
12. Ramakrishna, S.; Adepu, S. Controlled Drug Delivery Systems: Current Status and Future Directions. *Molecules* **2021**, *26*, 45.
13. Chopra, L.; Thakur, K.K.; Chohan, J.S.; Sharma, S.; Ilyas, R.A.; Asyraf, M.R.M.; Zakaria, S.Z.S. Comparative Drug Release Investigations for Diclofenac Sodium Drug (DS) by Chitosan-Based Grafted and Crosslinked Copolymers. *Materials* **2022**, *15*, 2404. [[CrossRef](#)] [[PubMed](#)]
14. Ailincăi, D.; Agop, M.; Marinas, I.C.; Zala, A.; Irimiciuc, S.A.; Dobreci, L.; Petrescu, T.C.; Volovat, C. Theoretical Model for the Diclofenac Release from PEGylated Chitosan Hydrogels. *Drug Deliv.* **2021**, *28*, 261–271. [[CrossRef](#)] [[PubMed](#)]
15. Parhi, R. Drug Delivery Applications of Chitin and Chitosan: A Review. *Environ. Chem. Lett.* **2020**, *18*, 577–594. [[CrossRef](#)]
16. Ye, H.; Wang, K.; Zhao, J.; Lu, Q.; Wang, M.; Sun, B.; Shen, Y.; Liu, H.; Pané, S.; Chen, X.Z.; et al. In Situ Sprayed Nanovaccine Suppressing Exosomal PD-L1 by Golgi Apparatus Disorganization for Postsurgical Melanoma Immunotherapy. *ACS Nano* **2023**, *17*, 10637–10650. [[CrossRef](#)] [[PubMed](#)]
17. Fekri, M.H.; Soleymani, S.; Mehr, M.R.; Akbari-adergani, B. Synthesis and Characterization of Mesoporous ZnO/SBA-16 Nanocomposite: Its Efficiency as Drug Delivery System. *J. Non-Cryst. Solids* **2022**, *591*, 121512. [[CrossRef](#)]
18. Goscińska, J.; Olejnik, A.; Ejsmont, A.; Galarda, A.; Wuttke, S. Overcoming the Paracetamol Dose Challenge with Wrinkled Mesoporous Carbon Spheres. *J. Colloid Interface Sci.* **2021**, *586*, 673–682. [[CrossRef](#)]
19. Jusu, S.M.; Obayemi, J.D.; Salifu, A.A.; Nwazojie, C.C.; Uzonwanne, V.; Odusanya, O.S.; Soboyejo, W.O. Drug-Encapsulated Blend of PLGA-PEG Microspheres: In Vitro and In Vivo Study of the Effects of Localized/Targeted Drug Delivery on the Treatment of Triple-Negative Breast Cancer. *Sci. Rep.* **2020**, *10*, 14188. [[CrossRef](#)]
20. Rojas, S.; Carmona, F.J.; Maldonado, C.R.; Horcajada, P.; Hidalgo, T.; Serre, C.; Rodriguez, J.A.; Barea, E. Nanoscaled Zinc Pyrazolate Metal-Organic Frameworks as Drug-Delivery Systems. *Acta Crystallogr. Sect. A Found. Adv.* **2017**, *73*, C1190. [[CrossRef](#)]
21. Maranescu, B.; Visa, A. Applications of Metal-Organic Frameworks as Drug Delivery Systems. *Int. J. Mol. Sci.* **2022**, *23*, 4458. [[CrossRef](#)] [[PubMed](#)]
22. Simagina, A.A.; Polynski, M.V.; Vinogradov, A.V.; Pidko, E.A. Towards Rational Design of Metal-Organic Framework-Based Drug Delivery Systems. *Russ. Chem. Rev.* **2018**, *87*, 831–858. [[CrossRef](#)]
23. Liu, X.; Liang, T.; Zhang, R.; Ding, Q.; Wu, S.; Li, C.; Lin, Y.; Ye, Y.; Zhong, Z.; Zhou, M. Iron-Based Metal-Organic Frameworks in Drug Delivery and Biomedicine. *ACS Appl. Mater. Interfaces* **2021**, *13*, 9643–9655. [[CrossRef](#)] [[PubMed](#)]
24. Almáši, M.; Zeleňák, V.; Palotai, P.; Beňová, E.; Zeleňáková, A. Metal-Organic Framework MIL-101(Fe)-NH<sub>2</sub> Functionalized with Different Long-Chain Polyamines as Drug Delivery System. *Inorg. Chem. Commun.* **2018**, *93*, 115–120. [[CrossRef](#)]
25. Gordon, J.; Kazemian, H.; Rohani, S. MIL-53(Fe), MIL-101, and SBA-15 Porous Materials: Potential Platforms for Drug Delivery. *Mater. Sci. Eng. C* **2015**, *47*, 172–179. [[CrossRef](#)]
26. Zhao, S.; Li, Y.; Wang, M.; Chen, B.; Zhang, Y.; Sun, Y.; Chen, K.; Du, Q.; Jing, Z.; Jin, Y. Preparation of MIL-88A Micro/Nanocrystals with Different Morphologies in Different Solvents for Efficient Removal of Congo Red from Water: Synthesis, Characterization, and Adsorption Mechanisms. *Microporous Mesoporous Mater.* **2022**, *345*, 112241. [[CrossRef](#)]
27. Pang, D.; Wang, C.C.; Wang, P.; Liu, W.; Fu, H.; Zhao, C. Superior Removal of Inorganic and Organic Arsenic Pollutants from Water with MIL-88A(Fe) Decorated on Cotton Fibers. *Chemosphere* **2020**, *254*, 126829. [[CrossRef](#)]
28. Huo, J.B.; Yu, G. Layered Double Hydroxides Derived from MIL-88A(Fe) as an Efficient Adsorbent for Enhanced Removal of Lead (II) from Water. *Int. J. Mol. Sci.* **2022**, *23*, 14556. [[CrossRef](#)]
29. Fu, H.; Song, X.X.; Wu, L.; Zhao, C.; Wang, P.; Wang, C.C. Room-Temperature Preparation of MIL-88A as a Heterogeneous Photo-Fenton Catalyst for Degradation of Rhodamine B and Bisphenol a under Visible Light. *Mater. Res. Bull.* **2020**, *125*, 110806. [[CrossRef](#)]
30. Khandelwal, G.; Maria Joseph Raj, N.P.; Vivekananthan, V.; Kim, S.J. Biodegradable Metal-Organic Framework MIL-88A for Triboelectric Nanogenerator. *iScience* **2021**, *24*, 102064. [[CrossRef](#)]

31. Baati, T.; Njim, L.; Neffati, F.; Kerkeni, A.; Bouttemi, M.; Gref, R.; Najjar, M.F.; Zakhama, A.; Couvreur, P.; Serre, C.; et al. In Depth Analysis of the in Vivo Toxicity of Nanoparticles of Porous Iron(III) Metal-Organic Frameworks. *Chem. Sci.* **2013**, *4*, 1597–1607. [[CrossRef](#)]
32. Horcajada, P.; Serre, C.; Maurin, G.; Ramsahye, N.A.; Balas, F.; Vallet-Regí, M.; Sebban, M.; Taulelle, F.; Férey, G. Porous Metal-Organic-Framework Nanoscale Carriers as a Potential Platform for Drug Delivery and Imaging. *J. Am. Chem. Soc.* **2008**, *130*, 6774–6780. [[CrossRef](#)] [[PubMed](#)]
33. Hirschle, P.; Hirschle, C.; Böll, K.; Döblinger, M.; Höhn, M.; Tuffnell, J.M.; Ashling, C.W.; Keen, D.A.; Bennett, T.D.; Rädler, J.O.; et al. Tuning the Morphological Appearance of Iron(III) Fumarate: Impact on Material Characteristics and Biocompatibility. *Chem. Mater.* **2020**, *32*, 2253–2263. [[CrossRef](#)]
34. McKinlay, A.C.; Eubank, J.F.; Wuttke, S.; Xiao, B.; Wheatley, P.S.; Bazin, P.; Lavalley, J.C.; Daturi, M.; Vimont, A.; De Weireld, G.; et al. Nitric Oxide Adsorption and Delivery in Flexible MIL-88(Fe) Metal-Organic Frameworks. *Chem. Mater.* **2013**, *25*, 1592–1599. [[CrossRef](#)]
35. Kim, S.N.; Park, C.G.; Huh, B.K.; Lee, S.H.; Min, C.H.; Lee, Y.Y.; Kim, Y.K.; Park, K.H.; Choy, Y. Bin Metal-Organic Frameworks, NH<sub>2</sub>-MIL-88(Fe), as Carriers for Ophthalmic Delivery of Brimonidine. *Acta Biomater.* **2018**, *79*, 344–353. [[CrossRef](#)] [[PubMed](#)]
36. Darvishi, S.; Javanbakht, S.; Heydari, A.; Kazeminava, F.; Gholizadeh, P.; Mahdipour, M.; Shaabani, A. Ultrasound-Assisted Synthesis of MIL-88(Fe) Coordinated to Carboxymethyl Cellulose Fibers: A Safe Carrier for Highly Sustained Release of Tetracycline. *Int. J. Biol. Macromol.* **2021**, *181*, 937–944. [[CrossRef](#)] [[PubMed](#)]
37. Illes, B.; Wuttke, S.; Engelke, H. Liposome-Coated Iron Fumarate Metal-Organic Framework Nanoparticles for Combination Therapy. *Nanomaterials* **2017**, *7*, 351. [[CrossRef](#)]
38. Kołodziejewska, J.; Kołodziejczyk, M. Diclofenac in the Treatment of Pain in Patients with Rheumatic Diseases. *Reumatologia* **2018**, *56*, 174–183. [[CrossRef](#)]
39. Ortiz, J.A.; Sepúlveda, F.A.; Panadero-Medianero, C.; Murgas, P.; Ahumada, M.; Palza, H.; Matsuhira, B.; Zapata, P.A. Cytocompatible Drug Delivery Hydrogels Based on Carboxymethylagarose/Chitosan PH-Responsive Polyelectrolyte Complexes. *Int. J. Biol. Macromol.* **2022**, *199*, 96–107. [[CrossRef](#)]
40. Amanullah, A.; Upadhyay, A.; Dhiman, R.; Singh, S.; Kumar, A.; Ahirwar, D.K.; Gutti, R.K.; Mishra, A. Development and Challenges of Diclofenac-Based Novel Therapeutics: Targeting Cancer and Complex Diseases. *Cancers* **2022**, *14*, 4385. [[CrossRef](#)]
41. Elmas, A.; Akyüz, G.; Bergal, A.; Andaç, M.; Andaç, Ö. Mathematical Modelling of Drug Release. *Res. Eng. Struct. Mater.* **2020**, *6*, 327–350. [[CrossRef](#)]
42. Available online: <https://www.originlab.com/> (accessed on 2 March 2020).
43. Liao, X.; Wang, F.; Wang, F.; Cai, Y.; Yao, Y.; Teng, B.T.; Hao, Q.; Shuxiang, L. Synthesis of (100) Surface Oriented MIL-88A-Fe with Rod-like Structure and Its Enhanced Fenton-like Performance for Phenol Removal. *Appl. Catal. B Environ.* **2019**, *259*, 118064. [[CrossRef](#)]
44. Jeong, H.; Lee, J. 3D-Superstructured Networks Comprising Fe-MIL-88A Metal-Organic Frameworks under Mechanochemical Conditions. *Eur. J. Inorg. Chem.* **2019**, *2019*, 4597–4600. [[CrossRef](#)]
45. Amaro-Gahete, J.; Klee, R.; Esquivel, D.; Ruiz, J.R.; Jiménez-Sanchidrián, C.; Romero-Salguero, F.J. Fast Ultrasound-Assisted Synthesis of Highly Crystalline MIL-88A Particles and Their Application as Ethylene Adsorbents. *Ultrason. Sonochem.* **2019**, *50*, 59–66. [[CrossRef](#)]
46. Melchiorre, M.; Lentini, D.; Cuccioli, M.E.; Taddeo, F.; Hmoudah, M.; Di Serio, M.; Ruffo, F.; Russo, V.; Esposito, R. Sustainable Ketalization of Glycerol with Ethyl Levulinate Catalyzed by the Iron(III)-Based Metal-Organic Framework MIL-88A. *Molecules* **2022**, *27*, 7229. [[CrossRef](#)] [[PubMed](#)]
47. Wang, J.; Wan, J.; Ma, Y.; Wang, Y.; Pu, M.; Guan, Z. Metal-Organic Frameworks MIL-88A with Suitable Synthesis Conditions and Optimal Dosage for Effective Catalytic Degradation of Orange G through Persulfate Activation. *RSC Adv.* **2016**, *6*, 112502–112511. [[CrossRef](#)]
48. Walshe, C.A.; Thom, A.J.R.; Wilson, C.; Ling, S.; Forgan, R.S. Controlling the Flexibility of MIL-88A(Sc) Through Synthetic Optimisation and Postsynthetic Halogenation. *Chem. Eur. J.* **2022**, *28*, e202201364. [[CrossRef](#)]
49. Butova, V.V.; Aboraia, A.M.; Shapovalov, V.V.; Dzhangiryan, N.A.; Papkovskaya, E.D.; Ilin, O.I.; Kubrin, S.P.; Guda, A.A.; Soldatov, A.V. Iron (II) Fluoride Cathode Material Derived from MIL-88A. *J. Alloys Compd.* **2022**, *916*, 165438. [[CrossRef](#)]
50. Chalati, T.; Horcajada, P.; Gref, R.; Couvreur, P.; Serre, C. Optimisation of the Synthesis of MOF Nanoparticles Made of Flexible Porous Iron Fumarate MIL-88A. *J. Mater. Chem.* **2011**, *21*, 2220–2227. [[CrossRef](#)]
51. Chameh, B.; Moradi, M.; Hajati, S.; Hessari, F.A.; Kiani, M.A. Morphology Control of Ni Doped Rod like MIL-88A Derived FeS<sub>2</sub> Embedded in Nitrogen-Rich Carbon as an Efficient Electrocatalyst for the Oxygen Reduction Reaction. *J. Mol. Struct.* **2021**, *1237*, 130329. [[CrossRef](#)]
52. Jiang, S.; Zhao, Z.; Chen, J.; Yang, Y.; Ding, C.; Yang, Y.; Wang, Y.; Liu, N.; Wang, L.; Zhang, X. Recent Research Progress and Challenges of MIL-88(Fe) from Synthesis to Advanced Oxidation Process. *Surf. Interfaces* **2022**, *30*, 101843. [[CrossRef](#)]
53. Rabeie, B.; Mahmoodi, N.M.; Mahkam, M. Morphological Diversity Effect of Graphene Quantum Dot/MIL88A(Fe) Composites on Dye and Pharmaceuticals (Tetracycline and Doxycycline) Removal. *J. Environ. Chem. Eng.* **2022**, *10*, 108321. [[CrossRef](#)]
54. Cheng, X.; Zhang, A.; Hou, K.; Liu, M.; Wang, Y.; Song, C.; Zhang, G.; Guo, X. Size- and Morphology-Controlled NH<sub>2</sub>-MIL-53(Al) Prepared in DMF-Water Mixed Solvents. *Dalt. Trans.* **2013**, *42*, 13698–13705. [[CrossRef](#)] [[PubMed](#)]

55. El Asmar, R.; Baalbaki, A.; Abou Khalil, Z.; Naim, S.; Bejjani, A.; Ghauch, A. Iron-Based Metal Organic Framework MIL-88-A for the Degradation of Naproxen in Water through Persulfate Activation. *Chem. Eng. J.* **2021**, *405*, 126701. [[CrossRef](#)]
56. Hmoudah, M.; El-Qanni, A.; Tesser, R.; Esposito, R.; Petrone, A.; Jung, O.S.; Salmi, T.; Russo, V.; Di Serio, M. Assessment of the Robustness of MIL-88A in an Aqueous Solution: Experimental and DFT Investigations. *Mater. Sci. Eng. B Solid-State Mater. Adv. Technol.* **2023**, *288*, 116179. [[CrossRef](#)]
57. Zhao, S.; Li, Y.; Wang, M.; Chen, B.; Zhang, Y.; Sun, Y.; Chen, K.; Du, Q.; Wang, Y.; Pi, X.; et al. Efficient Adsorption of Congo Red by Micro/Nano MIL-88A (Fe, Al, Fe-Al)/Chitosan Composite Sponge: Preparation, Characterization, and Adsorption Mechanism. *Int. J. Biol. Macromol.* **2023**, *239*, 124157. [[CrossRef](#)] [[PubMed](#)]
58. Gao, W.; Mu, B.; Zhu, Y.; Wang, A. Preparation of Palygorskite/MIL-88A(Fe) Composites for High-Efficient Removal of Congo Red. *Appl. Clay Sci.* **2023**, *242*, 107003. [[CrossRef](#)]
59. Chen, D.; Chen, S.; Jiang, Y.; Xie, S.; Quan, H.; Hua, L.; Luo, X.; Guo, L. Heterogeneous Fenton-like Catalysis of Fe-MOF Derived Magnetic Carbon Nanocomposites for Degradation of 4-Nitrophenol. *RSC Adv.* **2017**, *7*, 49024–49030. [[CrossRef](#)]
60. Bagherzadeh, E.; Zebarjad, S.M.; Hosseini, H.R.M. Morphology Modification of the Iron Fumarate MIL-88A Metal-Organic Framework Using Formic Acid and Acetic Acid as Modulators. *Eur. J. Inorg. Chem.* **2018**, *2018*, 1909–1915. [[CrossRef](#)]
61. Medvedev, P.V.; Butova, V.V.; Soldatov, M.A.; Kuzharov, A.A.; Fedorenko, A.G.; Shapovalova (Cherkasova), S.O.; Burachevskaya, O.A.; Gorban, I.E.; Soldatov, A.V. The Influence of Acetic Acid on the Properties of Microporous Metal-Organic Framework MIL-88a at Microfluidic Conditions and Room Temperature. *Nanobiotechnol. Rep.* **2021**, *16*, 488–496. [[CrossRef](#)]
62. Ren, G.; Zhao, K.; Zhao, L. A Fenton-like Method Using ZnO Doped MIL-88A for Degradation of Methylene Blue Dyes. *RSC Adv.* **2020**, *10*, 39973–39980. [[CrossRef](#)] [[PubMed](#)]
63. Ghodsinia, S.S.E.; Eshghi, H.; Mohammazinehad, A. Synthesis of Double-Shelled Periodic Mesoporous Organosilica Nanospheres/MIL-88A-Fe Composite and Its Elevated Performance for Pb<sup>2+</sup> Removal in Water. *Sci. Rep.* **2023**, *13*, 8092. [[CrossRef](#)] [[PubMed](#)]
64. Alipanah, N.; Yari, H.; Mahdavian, M.; Ramezanzadeh, B.; Bahlakeh, G. MIL-88A (Fe) Filler with Duplicate Corrosion Inhibitive/Barrier Effect for Epoxy Coatings: Electrochemical, Molecular Simulation, and Cathodic Delamination Studies. *J. Ind. Eng. Chem.* **2021**, *97*, 200–215. [[CrossRef](#)]
65. Ashrafi, M.; Farhadi, S. Polyoxometalate Supported on a Magnetic Fe<sub>3</sub>O<sub>4</sub>/MIL-88A Rod-like Nanocomposite as an Adsorbent for the Removal of Ciprofloxacin, Tetracycline and Cationic Organic Dyes from Aqueous Solutions. *RSC Adv.* **2023**, *13*, 6356–6367. [[CrossRef](#)] [[PubMed](#)]
66. Andrew Lin, K.Y.; Chang, H.A.; Hsu, C.J. Iron-Based Metal Organic Framework, MIL-88A, as a Heterogeneous Persulfate Catalyst for Decolorization of Rhodamine B in Water. *RSC Adv.* **2015**, *5*, 32520–32530. [[CrossRef](#)]
67. Tan, L.S.; Tan, H.L.; Deekonda, K.; Wong, Y.Y.; Muniyandy, S.; Hashim, K.; Pushpamalar, J. Fabrication of Radiation Cross-Linked Diclofenac Sodium Loaded Carboxymethyl Sago Pulp/Chitosan Hydrogel for Enteric and Sustained Drug Delivery. *Carbohydr. Polym. Technol. Appl.* **2021**, *2*, 100084. [[CrossRef](#)]
68. Fayrouz, D.; Abdallah, D.; Aicha, H. Experimental Investigation of Ternary Mixture of Diclofenac Sodium with Pharmaceutical Excipients. *Phys. Sci. Rev.* **2021**, *8*, 763–774. [[CrossRef](#)]
69. Kozakevych, R.B.; Bolbukh, Y.M.; Tertykh, V.A. Controlled Release of Diclofenac Sodium from Silica-Chitosan Composites. *World J. Nano Sci. Eng.* **2013**, *03*, 69–78. [[CrossRef](#)]
70. Crişan, A.G.; Porfire, A.; Iurian, S.; Rus, L.M.; Lucăcel Ciceo, R.; Turza, A.; Tomuță, I. Development of a Bilayer Tablet by Fused Deposition Modeling as a Sustained-Release Drug Delivery System. *Pharmaceuticals* **2023**, *16*, 1321. [[CrossRef](#)]
71. Ptaszowska-Koniarz, M.; Goscińska, J.; Pietrzak, R. Synthesis of Carbon Xerogels Modified with Amine Groups and Copper for Efficient Adsorption of Caffeine. *Chem. Eng. J.* **2018**, *345*, 13–21. [[CrossRef](#)]
72. Troyano, J.; Carné-Sánchez, A.; Pérez-Carvajal, J.; León-Reina, L.; Imaz, I.; Cabeza, A.; Maspoch, D. A Self-Folding Polymer Film Based on Swelling Metal-Organic Frameworks. *Angew. Chem. Int. Ed.* **2018**, *57*, 15420–15424. [[CrossRef](#)] [[PubMed](#)]
73. Lin, R.B.; Chen, B. Hydrogen-Bonded Organic Frameworks: Chemistry and Functions. *Chem* **2022**, *8*, 2114–2135. [[CrossRef](#)]
74. Li, Y.; Sui, J.; Cui, L.S.; Jiang, H.L. Hydrogen Bonding Regulated Flexibility and Disorder in Hydrazone-Linked Covalent Organic Frameworks. *J. Am. Chem. Soc.* **2023**, *145*, 1359–1366. [[CrossRef](#)]
75. Kundu, T.; Wahiduzzaman, M.; Shah, B.B.; Maurin, G.; Zhao, D. Solvent-Induced Control over Breathing Behavior in Flexible Metal-Organic Frameworks for Natural-Gas Delivery. *Angew. Chem.* **2019**, *131*, 8157–8161. [[CrossRef](#)]
76. Bui, A.; Guillen, S.G.; Sua, A.; Nguyen, T.C.; Ruiz, A.; Carachure, L.; Weber, M.D.R.; Cortez, A.; Tian, F. Iron-Containing Metal-Organic Framework Thin Film as a Drug Delivery System. *Colloids Surf. A Physicochem. Eng. Asp.* **2022**, *650*, 129611. [[CrossRef](#)] [[PubMed](#)]
77. Correa-Navarro, Y.M.; Moreno-Piraján, J.C.; Giraldo, L. Competitive Adsorption of Caffeine and Diclofenac Sodium onto Biochars Derived from Fique Bagasse: An Immersion Calorimetry Study. *ACS Omega* **2022**, *8*, 1967–1978. [[CrossRef](#)] [[PubMed](#)]
78. Zhang, M.; Wang, W.; Zhang, Q.; Deng, S. Pore Surface Engineering of Covalent Organic Frameworks by Simultaneously Appending Amine Group and Tailoring Pore Size for Efficient Adsorption of Diclofenac Sodium. *Chem. Eng. J.* **2023**, *459*, 141561. [[CrossRef](#)]
79. Bajpai, S.K.; Bhowmik, M. Adsorption of Diclofenac Sodium from Aqueous Solution Using Polyaniline as a Potential Sorbent. I. Kinetic Studies. *J. Appl. Polym. Sci.* **2010**, *117*, 3615–3622. [[CrossRef](#)]

80. Yuan, R.; Qiu, J.; Yue, C.; Shen, C.; Li, D.; Zhu, C.; Liu, F.; Li, A. Self-Assembled Hierarchical and Bifunctional MIL-88A(Fe)@ZnIn<sub>2</sub>S<sub>4</sub> Heterostructure as a Reusable Sunlight-Driven Photocatalyst for Highly Efficient Water Purification. *Chem. Eng. J.* **2020**, *401*, 126020. [[CrossRef](#)]
81. Barczak, M.; Dobrowolski, R.; Borowski, P.; Giannakoudakis, D.A. Pyridine-, Thiol- and Amine-Functionalized Mesoporous Silicas for Adsorptive Removal of Pharmaceuticals. *Microporous Mesoporous Mater.* **2020**, *299*, 110132. [[CrossRef](#)]
82. Weidner, E.; Barczak, P.; Goscianska, J.; Jesionowski, T.; Jaroniec, M.; Ciesielczyk, F. Soft-Templating Synthesis of Mesoporous Alumina Enriched with Lanthana and Its Potential as Diclofenac Delivery System. *Microporous Mesoporous Mater.* **2023**, *351*, 112487. [[CrossRef](#)]
83. Lach, J.; Szymonik, A. Adsorption of Diclofenac Sodium from Aqueous Solutions on Commercial Activated Carbons. *Desalin. Water Treat.* **2020**, *186*, 418–429. [[CrossRef](#)]
84. Mao, N.; Huang, L.; Shuai, Q. Facile Synthesis of Porous Carbon for the Removal of Diclofenac Sodium from Water. *ACS Omega* **2019**, *4*, 15051–15060. [[CrossRef](#)] [[PubMed](#)]
85. Shamsudin, M.S.; Azha, S.F.; Sellaoui, L.; Badawi, M.; Bonilla-Petriciolet, A.; Ismail, S. Performance and Interactions of Diclofenac Adsorption Using Alginate/Carbon-Based Films: Experimental Investigation and Statistical Physics Modelling. *Chem. Eng. J.* **2022**, *428*, 131929. [[CrossRef](#)]
86. Younes, H.A.; Taha, M.; Mahmoud, R.; Mahmoud, H.M.; Abdelhameed, R.M. High Adsorption of Sodium Diclofenac on Post-Synthetic Modified Zirconium-Based Metal-Organic Frameworks: Experimental and Theoretical Studies. *J. Colloid Interface Sci.* **2022**, *607*, 334–346. [[CrossRef](#)] [[PubMed](#)]
87. Prasetya, N.; Wöll, C. Removal of Diclofenac by Adsorption Process Studied in Free-Base Porphyrin Zr-Metal Organic Frameworks (Zr-MOFs). *RSC Adv.* **2023**, *13*, 22998–23009. [[CrossRef](#)] [[PubMed](#)]
88. Prasetya, N.; Li, K. MOF-808 and Its Hollow Fibre Adsorbents for Efficient Diclofenac Removal. *Chem. Eng. J.* **2021**, *417*, 129216. [[CrossRef](#)]
89. Sharma, A.; Rathore, V.K.; Chakraborty, M. Adsorptive Removal of Diclofenac Sodium from Aqueous Solution by Highly Efficient Metal Organic Framework (UiO-66)/Multi-Walled Carbon Nanotube Composite. *Environ. Sci. Pollut. Res.* **2023**, 1–14. [[CrossRef](#)]
90. Pournara, A.D.; Andreou, E.K.; Armatas, G.S.; Manos, M.J. Zirconium(IV) Metal Organic Frameworks with Highly Selective Sorption for Diclofenac under Batch and Continuous Flow Conditions. *Crystals* **2022**, *12*, 424. [[CrossRef](#)]
91. Li, H.Z.; Yang, C.; Qian, H.L.; Yan, X.P. Room-Temperature Synthesis of Ionic Covalent Organic Frameworks for Efficient Removal of Diclofenac Sodium from Aqueous Solution. *Sep. Purif. Technol.* **2023**, *306*, 122704. [[CrossRef](#)]
92. Huang, L.; Mao, N.; Yan, Q.; Zhang, D.; Shuai, Q. Magnetic Covalent Organic Frameworks for the Removal of Diclofenac Sodium from Water. *ACS Appl. Nano Mater.* **2020**, *3*, 319–326. [[CrossRef](#)]
93. Liu, W.; Shen, X.; Han, Y.; Liu, Z.; Dai, W.; Dutta, A.; Kumar, A.; Liu, J. Selective Adsorption and Removal of Drug Contaminants by Using an Extremely Stable Cu(II)-Based 3D Metal-Organic Framework. *Chemosphere* **2019**, *215*, 524–531. [[CrossRef](#)] [[PubMed](#)]
94. Arabkhani, P.; Javadian, H.; Asfaram, A.; Ateia, M. Decorating Graphene Oxide with Zeolitic Imidazolate Framework (ZIF-8) and Pseudo-Boehmite Offers Ultra-High Adsorption Capacity of Diclofenac in Hospital Effluents. *Chemosphere* **2021**, *271*, 129610. [[CrossRef](#)] [[PubMed](#)]
95. Li, S.; Cui, J.; Wu, X.; Zhang, X.; Hu, Q.; Hou, X. Rapid in Situ Microwave Synthesis of Fe<sub>3</sub>O<sub>4</sub>@MIL-100(Fe) for Aqueous Diclofenac Sodium Removal through Integrated Adsorption and Photodegradation. *J. Hazard. Mater.* **2019**, *373*, 408–416. [[CrossRef](#)]
96. Zhuang, S.; Liu, Y.; Wang, J. Mechanistic Insight into the Adsorption of Diclofenac by MIL-100: Experiments and Theoretical Calculations. *Environ. Pollut.* **2019**, *253*, 616–624. [[CrossRef](#)] [[PubMed](#)]
97. Sharifian, S.; Farshchi Tabrizi, F.; Sardarian, A. Efficient Adsorptive Removal of Diclofenac Sodium by Acidified MIL101(Cr): Optimizing the Content of Phosphotungstic Acid, Flow Loop Thin Film Slurry Flat Plate Reactor. *J. Porous Mater.* **2023**, *30*, 975–988. [[CrossRef](#)]
98. Goscianska, J.; Marciniak, M.; Pietrzak, R. Ordered Mesoporous Carbons Modified with Cerium as Effective Adsorbents for Azo Dyes Removal. *Sep. Purif. Technol.* **2015**, *154*, 236–245. [[CrossRef](#)]
99. Kalam, S.; Abu-Khamsin, S.A.; Kamal, M.S.; Patil, S. Surfactant Adsorption Isotherms: A Review. *ACS Omega* **2021**, *6*, 32342–32348. [[CrossRef](#)]
100. Marciniak, M.; Goscianska, J.; Norman, M.; Jesionowski, T.; Bazan-Wozniak, A.; Pietrzak, R. Equilibrium, Kinetic, and Thermodynamic Studies on Adsorption of Rhodamine B from Aqueous Solutions Using Oxidized Mesoporous Carbons. *Materials* **2022**, *15*, 5573. [[CrossRef](#)]
101. Alves, R.C.; Lucena, G.N.; de Farias, R.L.; da Silva, P.B.; da Silva, I.C.; Pavan, F.R.; Chorilli, M.; da Costa Ferreira, A.M.; Galvão Frem, R.C. Copper(II) Biocompatible Coordination Solids as Potential Platforms for Diclofenac Delivery Systems. *J. Solid State Chem.* **2020**, *289*, 121479. [[CrossRef](#)]
102. Kumar, V.; Kaur, G.; Pickrell, G.R. Silica Nanospheres. *Biomed. Ther. Clin. Appl. Bioact. Glas.* **2018**, 521–544. [[CrossRef](#)]
103. Zheng, M.; Chen, J.; Zhang, L.; Cheng, Y.; Lu, C.; Liu, Y.; Singh, A.; Trivedi, M.; Kumar, A.; Liu, J. Metal Organic Frameworks as Efficient Adsorbents for Drugs from Wastewater. *Mater. Today Commun.* **2022**, *31*, 103514. [[CrossRef](#)]
104. Ding, H.; Li, B.; Jiang, Y.; Liu, G.; Pu, S.; Feng, Y.; Jia, D.; Zhou, Y. PH-Responsive UV Crosslinkable Chitosan Hydrogel via “Thiol-Ene” Click Chemistry for Active Modulating Opposite Drug Release Behaviors. *Carbohydr. Polym.* **2021**, *251*, 117101. [[CrossRef](#)] [[PubMed](#)]

105. Lei, X.; Zhou, Y.; Liu, X.; Kong, L.; Liao, L.; Li, Y.; Liu, M.; Tian, L.; Rao, W.; Lv, G. Effective PH-Responsive Nanocarrier Based on the Anisotropic Surfaces of Halloysite Nanotubes for Controlled Drug Release. *Appl. Clay Sci.* **2023**, *232*, 106799. [[CrossRef](#)]
106. Wang, S.-y.; Li, J.; Zhou, Y.; Li, D.-Q.; Du, G.-M. Chemical Cross-Linking Approach for Prolonging Diclofenac Sodium Release from Pectin-Based Delivery System. *Int. J. Biol. Macromol.* **2019**, *137*, 512–520. [[CrossRef](#)] [[PubMed](#)]
107. Zauska, L.; Bova, S.; Benova, E.; Bednarcik, J.; Balaz, M.; Zelenak, V.; Hornebecq, V.; Almasi, M. Thermosensitive Drug Delivery System SBA-15-PEI for Controlled Release of Nonsteroidal Anti-Inflammatory Drug Diclofenac Sodium Salt: A Comparative Study. *Materials* **2021**, *14*, 1880. [[CrossRef](#)] [[PubMed](#)]
108. Nikolova, D.; Simeonov, M.; Tzachev, C.; Apostolov, A.; Christov, L.; Vassileva, E. Polyelectrolyte Complexes of Chitosan and Sodium Alginate as a Drug Delivery System for Diclofenac Sodium. *Polym. Int.* **2022**, *71*, 668–678. [[CrossRef](#)]
109. Vargas, A.M.; Cipagauta-Ardila, C.C.; Molina-Velasco, D.R.; Ríos-Reyes, C.A. Surfactant-Modified Natural Zeolites as Carriers for Diclofenac Sodium Release: A Preliminary Feasibility Study for Pharmaceutical Applications. *Mater. Chem. Phys.* **2020**, *256*, 123644. [[CrossRef](#)]
110. Lucena, G.N.; Alves, R.C.; Abuçafy, M.P.; Chiavacci, L.A.; da Silva, I.C.; Pavan, F.R.; Frem, R.C.G. Zn-Based Porous Coordination Solid as Diclofenac Sodium Carrier. *J. Solid State Chem.* **2018**, *260*, 67–72. [[CrossRef](#)]
111. Simon, M.A.; Anggraeni, E.; Soetaredjo, F.E.; Santoso, S.P.; Irawaty, W.; Thanh, T.C.; Hartono, S.B.; Yuliana, M.; Ismadji, S. Hydrothermal Synthesize of HF-Free MIL-100(Fe) for Isoniazid-Drug Delivery. *Sci. Rep.* **2019**, *9*, 16907. [[CrossRef](#)]
112. Shafiei, F.; Ghavami-Lahiji, M.; Kashi, T.J.; Najafi, F. Drug Release Kinetics and Biological Properties of a Novel Local Drug Carrier System. *Dent. Res. J.* **2021**, *18*, 94. [[CrossRef](#)]
113. Paarakh, M.P.; Jose, P.A.; Setty, C.M.; Christopher, G.V. Release Kinetics—Concepts and Applications. *Int. J. Pharm. Res. Technol.* **2018**, *8*, 12–20. [[CrossRef](#)]
114. Biswas, G.R.; Bhattacharya, S.; Ghoshal, P.; Majee, S.B. Fabrication of Microsponge as Drug Delivery of an Antihypertensive Drug. *Eur. J. Pharm. Med. Res.* **2020**, *7*, 423–430.

**Disclaimer/Publisher's Note:** The statements, opinions and data contained in all publications are solely those of the individual author(s) and contributor(s) and not of MDPI and/or the editor(s). MDPI and/or the editor(s) disclaim responsibility for any injury to people or property resulting from any ideas, methods, instructions or products referred to in the content.